The current issue and full text archive of this journal is available at
www.emeraldinsight.com/0961-5539.htm

Lattice-BGK simulation of steady flow through vascular tubes with double constrictions

Haibo Huang, T.S. Lee and C. Shu
Fluid Division, Department of Mechanical Engineering, National University of Singapore, Singapore

Received September 2004
Reviewed April 2005
Accepted April 2005

Abstract

Purpose – The aim of the present study is to evaluate the accuracy and efficiency of Lattice-BGK (LBGK) method application in simulation of the 3D flow through complex geometry. On the other hand, the steady flows through vascular tube with Reynolds number 10-150 and different constriction spacing ratios are simulated.

Design/methodology/approach – The numerical method is based on the LGBK method with an incompressible D3Q19 model. To treat the curved boundary, the "bounce back" scheme combined with spatial interpolation of second order is applied.

Findings – The highly axisymmetric property in the direct 3D tube flow simulation is observed. Solutions obtained from LBGK method are quite consistent with that of finite volume method (FVM). The overall order of accuracy of these LBGK solutions is about 1.89. The LBGK incompressible D3Q19 model with the curved boundary treatment can handle the problems of 3D steady flow through complex geometry.

Research limitations/implications – Investigating the flow in constricted vascular tubes with different stenose shape and higher Reynolds number is left for future work.

Practical implications – Lattice BGK method is the very useful tool to investigate the steady vascular flow.

Originality/value – Applying LBGK method with incompressible D3Q19 model to simulate the steady flow through complex geometry. The accuracy and efficiency of the present LBGK solver are examined.

Keywords Numerical analysis, Flow, Body fluids

Paper type Research paper

1. Introduction

The lattice Boltzmann method (LBM) has been proposed as an alternative numerical scheme for solving the Navier-Stokes (NS) equations. Historically, the LBM was developed from the method of Lattice-gas Automata. Since McNamara and Zanetti (1988) used Boltzmann equation to simulate lattice-gas Automata, LBM has been developed very rapidly (Higuera and Jimenez, 1989; Chen *et al.*, 1992a, b; He *et al.*, 1996; Mei *et al.*, 1999; Yu *et al.*, 2003). Unlike traditional finite difference method and finite volume method (FVM), LBM based on the microscopic kinetic equation for the particle distribution function and from the function, the macroscopic quantities can be obtained. The kinetic nature provides LBM some merits. Firstly, it is easy to program. Since the simple collision step and streaming step can recover the non-linear macroscopic advection, basically, only a loop of the two simple steps is implemented in LBM programs. Secondly, the simple pressure density relationship matches well with

International Journal of Numerical Methods for Heat & Fluid Flow
Vol. 16 No. 2, 2006
pp. 185-203

0961-5539
DOI 10.1108/09615530610644262

current trends of parallel computing (Chen *et al.*, 1996). Thirdly, LBM seeks for the minimum set of velocities in phase space. Actually, only one or two speeds and a few moving directions are used in LBM velocity model, for example, commonly used 3D 19-velocity model (D3Q19) has two speeds and 18 moving directions. For the approaches in LBM, Lattice Bhatnagar-Gross-Krook (LBGK) scheme is the simplest approach because it only has a scalar relaxation parameter τ. For its simplicity, here the LBGK method is employed to simulate the steady viscous flow in vascular tubes.

The flow in constricted tubes has been of great interest to biodynamicists because localized arterial stenoses may occur in the cardiovascular system which due to atherosclerosis. The stenoses may affect the cardiovascular system severely because Young and Tsai (1973) found that when the internal diameter is reduced beyond about 50 per cent of the nominal value, the pressure losses may be significant. In the past, there are many numerical studies on steady laminar flow in axisymmetric constricted tubes. Lee (1990, 1994) applied the vorticity-stream function approach to study the laminar flow through variable constrictions in vascular tube. Through study in Reynolds numbers 5-200, Lee (1990, 1994) mainly addressed the effect of the different constriction spacing ratios. Damodaran *et al.* (1996) studied the laminar flow through tubes with multiple constrictions by FVM.

Recently, using LBM to investigation of 2D constricted channel flow or 3D tube flow become more popular. For 2D channel flow, Luo (1997) deals with some flow in 2D symmetric channel with expansion. Cosgrove *et al.* (2003) studied the transition of oscillatory channel flow. For 3D flow in rigid straight tubes, Halliday *et al.* (2001) simulated the axis-symmetric flow by using LBGK D2Q9 model and adding an extra term into an adjusted evaluation equation for the lattice fluid's momentum distribution. However, the extra term added into the evaluation equation involves stress and high order fluxes, the finite difference can not be avoid which may destroy the spirit of the LBM.

Hence, many studies (Chen *et al.*, 1992a, b; Maier *et al.*, 1996; Mei *et al.*, 2000; Artoli *et al.*, 2002) about the flows in circular tube still have to recourse to 3D LBM model. Usually, three athermal 3D Lattice Boltzmann Equation (LBE) models (D3Q15, D3Q19, and D3Q27) are available. Because the D3Q19 model provides a balance between computational reliability and efficiency comparing with the D3Q15 model and the D3Q27 model (Mei *et al.*, 2000), we apply the D3Q19 velocity model in our simulation.

At beginning, Maier *et al.* (1996) simulated the poiseuille flow in a circular pipe by D3Q19 model with the bounce back scheme. Without an accurate curved boundary treatment, the boundaries must be represented by lattice nodes, hence the actual boundaries become jagged and the discretization error can decrease only by increasing lattice system.

Later, some more accurate curved boundary treatments were proposed and applied in simulation 3D circular tube flow. Mei *et al.* (2000) proposed an accurate 3D curvature boundary treatment and simulated 3D circular tube flow using the standard D3Q19 model. Artoli *et al.* (2002) using the standard D3Q19 model studied the 3D pulsatile flow in a pipe with the boundary treatment proposed by Bouzidi *et al.* (2001). However, Hou *et al.*(1995) and Maier *et al.* (1996) found that the calculations with pressure gradient are subject to compressibility error, which is due to the compressibility effect of standard D2Q9 and D3Q19 models. When using LBM, diminishing the compressibility effect is important for study pulsatile flow or flow with large

pressure gradient. Hence, He and Luo (1997) proposed an incompressible LBE model. Using the incompressible D3Q19 model, a few 3D cases such as the flow in lid-driven cavity (d'Humieres *et al.*, 2002) or natural convection of air in a cubical enclosure (Peng *et al.*, 2004) were performed. However, the cases are all with very simple geometry and not involve large pressure gradient.

Till today, studies of using incompressible D3Q19 model to simulate the flow through complex geometry with large pressure gradient have not been reported. One aim of our present study is to test LBGK method application in simulation of the 3D flow through complex geometry. Hence, the accuracy of LBGK solutions is evaluated and the efficiency of LBGK method is compared with that of FVM. On the other hand, because we are particularly interested in flow through vascular tube, we would like using LBGK method to investigate the effect of distance between two adjacent stenoses on streamlines, shear stress, etc. as the flow passes through them.

1.1 Stenotic vessel geometry and lattices

Geometry of the constrictions may be described by different profiles, such as the Gaussian distribution curve, Cosine curve, etc. Because the Cosine curve provides a smooth constriction which can represents an arterial stenose, Cosine curve is used in our study. The geometry of two stenoses is shown in Figure 1. If r_0 is the radius of the nonstenotic part of the tube, radius of the first stenose $r(x)$ is given in below function:

$$r(x) = r_0 - \beta r_0\{1 + \cos[2\pi(x - S_1)/D]\}/2 \quad (S_1 - D < x < S_1 + D)$$

where $r_0 = D/2$, $\beta = 50$ per cent is severity of stenose and the axial length of each stenose is $2D$. For the geometry of the second same stenose, parameter S_1 in above geometry function should be replaced with S_2. The distance of two stenoses is defined as $S = S_2 - S_1$.

To make flow fully developed and save grid nodes, length between the right end and the second stenose is $8D$, as shown in Figure 1. The total length $L = 11D + S$. In this paper, if not stated clearly, the lattices used are uniform with 43 lattices units in y and z direction and $(L*40 + 1)$ lattice units in x direction.

2. Numerical methods

2.1 Lattice-BGK (LBGK) method

It is well known that the standard LBGK D2Q9 and D3Q19 model involves the compressibility effect (Hou *et al.*, 1995; Artoli *et al.*, 2002). To solve any problem, when using LBM, the pressure changes are described by density variance. In our present

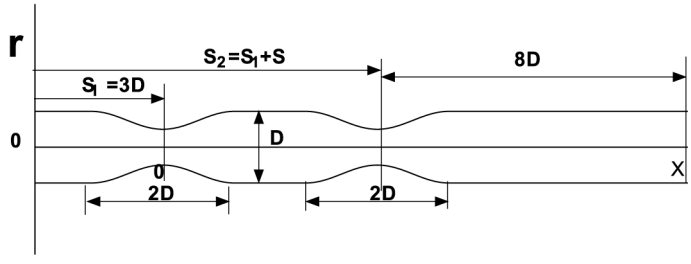

Figure 1.
Model of the double constriction tube (case $S/D = 3$)

study of viscous flow through constricted vascular tubes, the non-dimensional pressure drop $\Delta p/(\rho U^2)$ is equal to $c_s^2 \Delta\rho/(\rho U^2)$, where $c_s^2 = 1/3$ and U is the characteristic velocity (usually the maximum value of the inlet fully developed parabolic velocity profile). Hence, when using the standard D3Q19 model to simulate the flow involve high pressure drop, only very small U can be used to diminish the compressibility effects, which can be approximately evaluated by $\Delta\rho/\rho$. However, for certain Reynolds number, reducing U would make τ value very close to 0.5, which may lead to numerical instability. To solve the problem, the technique of increasing the mesh size is commonly used (He *et al.*, 1996), which may result in a much larger mesh system than conventional CFD methods such as FVM.

To overcome the above difficulties, He and Luo (1997) proposed an incompressible D2Q9 model used for steady and unsteady flows. Using the incompressible D2Q9 model, characteristic velocity $U < 0.15$ is valid and not necessary to adopt very small value.

In present study, we applied an incompressible D3Q19 model which is similar to the incompressible D2Q9 model proposed by He and Luo (1997). In LBGK method, $f_i(\mathbf{x}, t)$ is the distribution function for particles with velocity $\mathbf{e}_i$ at position $\mathbf{x} = (x, y, z)$ and time t. $\mathbf{u} = (u, v, w)$, u, v, w are x, y and z component velocities, respectively. The macroscopic pressure p and momentum $p_0\mathbf{u}$ are defined as:

$$\sum_{i=0}^{18} f_i = p, \quad \sum_{i=0}^{18} f_i \mathbf{e}_i = p_0 \mathbf{u} \tag{1}$$

where p_0 is the average pressure. For 3D 19 velocity model, it is written as:

$$\begin{matrix}[\mathbf{e}_0, \mathbf{e}_1, \mathbf{e}_2, \mathbf{e}_3, \mathbf{e}_4, \mathbf{e}_5, \mathbf{e}_6, \mathbf{e}_7, \mathbf{e}_8, \mathbf{e}_9, \mathbf{e}_{10}, \mathbf{e}_{11}, \mathbf{e}_{12}, \mathbf{e}_{13}, \mathbf{e}_{14}, \mathbf{e}_{15} \mathbf{e}_{16}, \mathbf{e}_{17}, \mathbf{e}_{18}]\end{matrix}$$
$$= \begin{bmatrix} 0 & 1 & -1 & 0 & 0 & 0 & 0 & 1 & 1 & -1 & -1 & 1 & -1 & 1 & -1 & 0 & 0 & 0 & 0 \\ 0 & 0 & 0 & 1 & -1 & 0 & 0 & 1 & -1 & 1 & -1 & 0 & 0 & 0 & 0 & 1 & 1 & -1 & -1 \\ 0 & 0 & 0 & 0 & 0 & 1 & -1 & 0 & 0 & 0 & 0 & 1 & 1 & -1 & -1 & 1 & -1 & 1 & -1 \end{bmatrix}$$

The velocity model is shown in Figure 2.

In Lattice BGK method, the two main steps implemented are collision and streaming. In the collision step:

$$f_i^{\mathrm{ne}} = f_i(\mathbf{x}, t) - f_i^{\mathrm{eq}}(\mathbf{x}, t) \tag{2a}$$

$$f_i(\mathbf{x}, t) = f_i^{\mathrm{eq}}(\mathbf{x}, t) + (1 - \frac{1}{\tau}) f_i^{\mathrm{ne}} \tag{2b}$$

where f_i^{ne} is the non-equilibrium term and the equilibrium function $f_i^{\mathrm{eq}}(\mathbf{x}, t)$ is defined as:

$$f_i^{\mathrm{eq}}(\mathbf{x}, t) = \alpha_i p + \alpha_i p_0 \left[\frac{\mathbf{e}_i \cdot \mathbf{u}}{c_s^2} + \frac{(\mathbf{e}_i \cdot \mathbf{u})^2}{2c_s^4} - \frac{\mathbf{u}^2}{2c_s^2} \right] \tag{3}$$

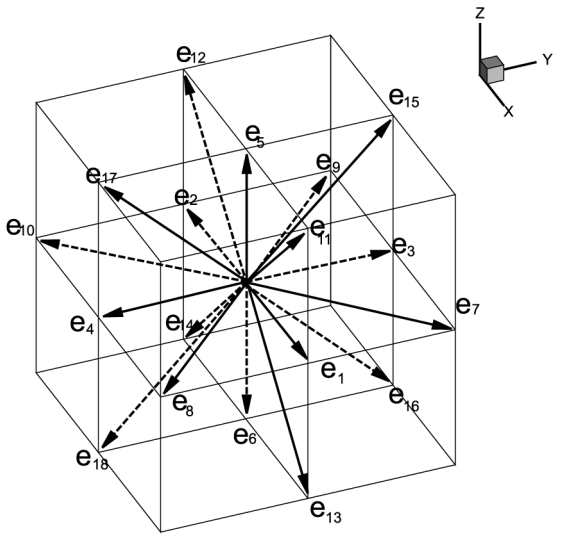

Figure 2.
Scheme of lattice model (3D 19 velocity model)

where $i = 0, 1, 2 \ldots, 18$ with $\alpha_0 = 1/3$, $\alpha_i = 1/18$, $(i = 1, 2, \ldots 6)$, $\alpha_i = 1/36$, $(i = 7, 8, \ldots 18)$ $c_s^2 = 1/3$.

It is noticed that the main difference between above LBGK incompressible D3Q19 model and the standard D3Q19 model is the form of equilibrium distribution function (He and Luo, 1997).

The relax time constant τ and the fluid viscosity ν satisfies equation $\nu = (2\tau - 1)\delta x/6$, where $\delta x = 1$ is the lattice space. In this paper, time step $\delta t = 1$.

In the streaming step, as standard LBGK, equation (4) is implemented on all lattices:

$$f_i(\mathbf{x} + \mathbf{e}_i, t + 1) = f_i^+(\mathbf{x}, t) \tag{4}$$

In the computation procedure, we would like to know the shear stress tensor since it is important in vascular flow study. For Lattice-BGK (LBGK) method, the shear stress σ_{xy} can be computed conveniently from equation (5):

$$\sigma_{xy} = -\left(1 - \frac{1}{2\tau}\right)\sum_{i=0}^{18} f_i^{(1)} \mathrm{e}_{ix}\mathrm{e}_{iy} = \rho\nu\left[\frac{\partial u}{\partial y} + \frac{\partial v}{\partial x}\right] \tag{5}$$

in lattice units, where:

$$\sum_{i=0}^{18} f_i^{(1)} \mathrm{e}_{ix}\mathrm{e}_{iy} = \sum_{i=0}^{18} (f_i - f_i^{\mathrm{eq}})\mathrm{e}_{ix}\mathrm{e}_{iy} + 0(\varepsilon^2) \tag{6}$$

Equation (5) is usually calculated after the collision step. Hence, actually, it is not necessary to pay additional computational cost to estimate the shear stress through the velocity field which is usually needed in other CFD method (Artoli *et al.*, 2002). The symbol $o(\varepsilon^2)$ means second order accuracy in space.

In our study, for defining steady state, our criterion is:

$$\sum_{i,j} \frac{\| \sqrt{[u(i,j,t+1) - u(i,j,t)]^2 + [v(i,j,t+1) - v(i,j,t)]^2} \|}{\| \sqrt{[u(i,j,t+1)]^2 + [v(i,j,t+1)]^2} \|} < 10^{-4} \quad (7)$$

where i, j are the lattice nodes in $z = 0$ plane and $u(i, j, t)$, $v(i, j, t)$ are x, y component velocity at time t, respectively.

2.2 Boundary condition

In general, according to the study of Chen *et al.* (1992a, b), the accuracy of the LBM is of second order in both time and space. However, Zou and He (1997) and He *et al.* (1997) found the wall boundary treatment may affect the overall accuracy. For example, the original bounce back scheme is only of first order in numerical accuracy. Later, some other boundary treatments were also proposed, such as the half way bounce back scheme (Ladd, 1994), the non-equilibrium bounce back scheme (Zou and He, 1997) and the extrapolation scheme (Chen *et al.*, 1996). They all can give out improved results. However, these treatments are most suitable for flat walls.

In 1998, an accurate curved wall boundary treatment was proposed by Filippova and Hanel (1998) and later improved by Mei *et al.* (1999). And later Mei *et al.* (2000) extended the 2D curved wall boundary treatment to 3D cases. Guo *et al.* (2002a, b) also proposed a curved wall boundary treatment based on the idea of Zou and He (1997). However, the most successful one was the treatment proposed by Bouzidi *et al.* (2001). It combined the "bounce back" scheme and spatial interpolation of second order. Mei *et al.* (2002) and Lallemand and Luo (2003) also found the boundary condition is a simple, robust, efficient and accurate scheme. In our study, this curved boundary treatment was uniformly applied to all near wall nodes.

The concept of the Bouzidi's curve boundary treatment is very simple. Here, we use a 2D problem to illustrate the idea. In Figure 3, q is defined as the fraction of the intersection link in the fluid region: $q = (|\mathbf{x}_f - \mathbf{x}_b|)/(|\mathbf{x}_f - \mathbf{x}_w|)$, where $\mathbf{x}_f$, $\mathbf{x}_b$ and $\mathbf{x}_w$ are positions of fluid node, boundary node and wall node, respectively. Because the collision step is not applicable to the wall nodes, for the fluid nod e which is most near to the wall nodes, the distribution functions in some direction are actually unknown for streaming step. For example, in Figure 3, for fluid node "j", distribution functions f_3, f_4, f_7 and f_6 are unknown.

Bouzidi *et al.* (2001) used a scheme to determine these unknowns. Firstly, the half way bounce-back boundary condition should be understood. In Figure 3, for case $q = 1/2$, the actual position of the wall is located at "b_3", which is about one-half grid spacing beyond the last fluid node "j". The distribution function $f_3(\mathbf{x}_j, t+1)$ can be obtained from a formula $f_3(\mathbf{x}_j, t+1) = f_1^+(\mathbf{x}_j, t)$, which means the particle with the velocity $\mathbf{e}_1$, travelled one grid spacing for one time step.

With the picture for the simple bounce-back scheme in mind, it is easy to understand the situation depicted for other cases. For case $q < 1/2$, at time t, the distribution function of the particle with velocity $\mathbf{e}_5$ at the point "c", which located at a distance $\sqrt{2}(1 - 2q)\delta x$ away from the grid point "j" would end up at the grid point "j" after bounce back collision. That is shown by the thick bent arrow in Figure 3. So, it is easy to obtain $f_7(\mathbf{x}_j, t+1)$ if we know $f_5^+(\mathbf{x}_c, t)$ because $f_7(\mathbf{x}_j, t+1) = f_5^+(\mathbf{x}_c, t)$. Although $\mathbf{x}_c$ is not a grid point, the value of $f_5^+(\mathbf{x}_c, t)$ at the point can be reconstructed

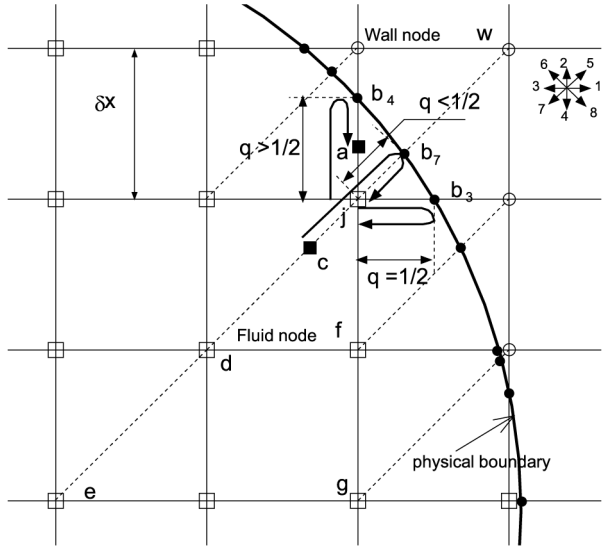

Notes: Open circles (○) are wall nodes and open squares (□) are the fluid nodes. The disks (●) are the nodes in physical boundary. Solid squares (■) are located in the fluid region but not on grid nodes. The thin solid lines are the grid lines. The thick arrows represent the trajectory of a particle interacting with the wall, described in Eqs. (8) and (9)

Figure 3.
Curved boundary geometry and lattice nodes

by a quadratic interpolation involving values of $f_5^+(\mathbf{x}_j, t)$, $f_5^+(\mathbf{x}_d, t)$ and $f_5^+(\mathbf{x}_e, t)$. In a similar manner, for the case of $q > 1/2$ shown in Figure 3, we can construct $f_4(\mathbf{x}_j, t+1)$ by a quadratic interpolation involving $f_4(\mathbf{x}_a, t+1)$, $f_4(\mathbf{x}_f, t+1)$ and $f_4(\mathbf{x}_g, t+1)$, where $f_4(\mathbf{x}_a, t+1) = f_2^+(\mathbf{x}_j, t)$. In this way, extrapolations in the boundary conditions are avoided for the sake of numerical stability. This leads to the following quadratic interpolation formulas.

For the case of $q < 1/2$:

$$f_7(\mathbf{x}_j, t+1) = q(1+2q)f_5^+(\mathbf{x}_j, t) + (1-4q^2)f_5^+(\mathbf{x}_d, t) - q(1-2q)f_5^+(\mathbf{x}_e, t) \quad (8)$$

For case $q > 1/2$, to get $f_4(\mathbf{x}_j, t+1)$,

$$f_4(\mathbf{x}_j, t+1) = \frac{1}{q(1+2q)}f_2^+(\mathbf{x}_j, t) + \frac{(2q-1)}{q}f_4(\mathbf{x}_f, t+1) - \frac{(2q-1)}{(2q+1)}f_4(\mathbf{x}_g, t+1) \quad (9)$$

Study of Lallemand and Luo (2003) provides more general formulas for moving and stationary boundary.

For the inlet and outlet boundary conditions, the extrapolation method proposed by Guo *et al.* (2002a, b) is applied. The fully developed Poiseuille parabolic velocity profile in the inlet boundary is specified and the corresponding pressure of the fluid is extrapolated from the next inner nodes. Then the equilibrium part of distribution function can be determined through equation (3). The corresponding non-equilibrium part of distribution function can be extrapolated from the next inner nodes. So the collision step can be implemented. The characteristic velocity U is chosen as 0.1 in our simulations. For the outlet boundary, the outlet pressure is

specified and corresponding velocity is extrapolated from the inner nodes. The equilibrium and non-equilibrium part of distribution functions determined in the same way as inlet boundary condition.

2.3 Finite volume Navier-Stokes (NS) Solver

For comparison purposes, a pressure-based finite-volume NS solver, FLUENT (a commercial software), is used in this study. When applying FLUENT, we set an implicit solver, which is relatively efficient in obtaining steady-state solutions.

The 3D unstructured linear brick element mesh is generated for FLUENT simulation. Also for comparison purposes, the number of the grid nodes is the same as the number of uniform grid nodes for LBM solver.

On the other hand, the LBM is a time-accurate explicit solver. The time step allowed is limited by stability constraint. Therefore, we should notice above difference between the two solvers when we compare their efficiency. Actually, some other studies (Noble *et al.*, 1996) have found that the LBM is as efficient as conventional methods when similar explicit time-marching schemes are used.

3. Results and discussion

In this part, viscous flows through constricted vascular tubes with different Reynolds number are simulated. Firstly, to validate our 3D LBGK solver, results of LBGK and FVM are presented and compared, and then followed by a detailed comparison of accuracy and efficiency between the two solvers. In the end of this part, the effect of distance between two adjacent stenoses on streamlines, shear stress, vorticity and velocity distribution as the flow passes through them are also discussed.

Firstly, we would like to validate our 3D LBGK solver. To investigate whether the flow is axis-symmetric is very interesting for such 3D simulation. Here, we defined a variable of state, χ, to measure the asymmetry (Luo, 1997):

$$\chi = \sum\nolimits_{\mathbf{x}_{i,j} \in \Omega} \left[u(\mathbf{x}_{i,j}) - u(\bar{\mathbf{x}}_{i,j}) \right]^2 \tag{10}$$

where Ω is one of the eight planes is shown in Figure 4. Plane i can be described in cylinder coordinate system by $\varphi = (i-1)\pi/4$, $(1 \le i \le 8)$. $\bar{\mathbf{x}}_{ij}$ is an axisymmetric node of $\mathbf{x}_{i,j}$. It is obvious that when the flow pattern is axisymmetric, $\chi = 0$. However, the value of χ, is not exactly zero when the system reaches its steady state, which depends on the system size in the simulation. Here, to investigate value of χ, simulations of the case $S/D = \infty$ (one constriction) with Reynolds number 10, 50 and 150 are performed. Through observation made with two lattice system sizes, $N_x \times N_y \times N_z = 221 \times 21 \times 21$ and $441 \times 41 \times 41$, it is found that the values of χ at the steady state decays to zero as N_x^{-3}.

And then, we would like to present and compare the results of LBGK and FVM. Appling the two solvers, simulations of the case $S/D = \infty$ (one constriction) with Reynolds number 10, 50 and 100 are performed. For simplicity, in all of the velocity profiles comparisons, due to axisymmetric velocity field, for results obtained from FVM, we only show the data along a radius.

From Figure 5, we can see that both the normalized axial and radial velocity component U, V profiles in different x positions of LBGK agree well with that of the

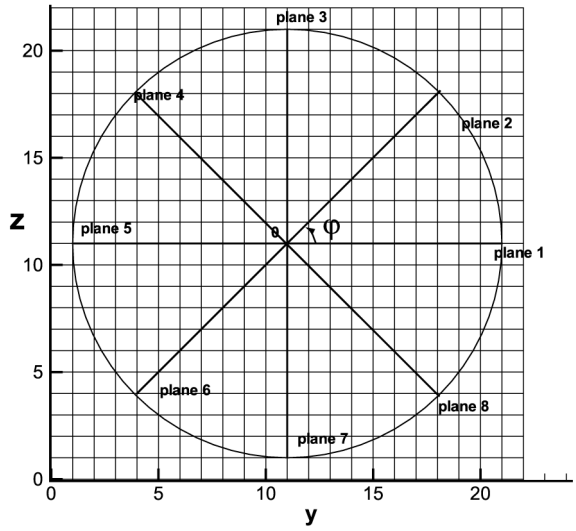

Figure 4.
u velocities in the 8 planes are investigated for asymmetry

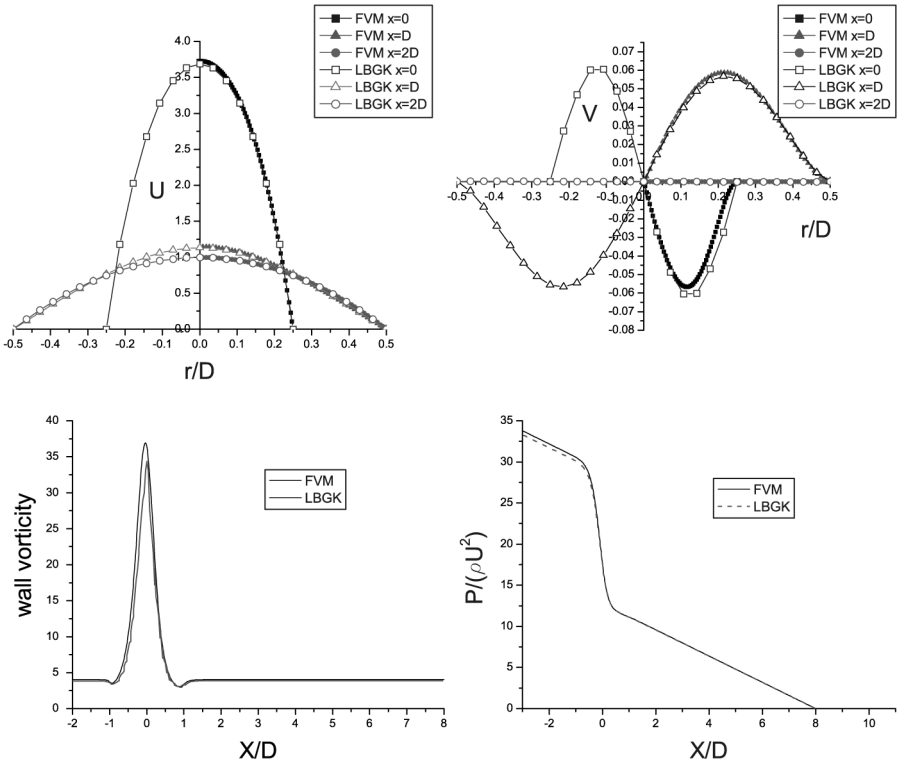

Figure 5.
Solutions of FVM and LBM ($S/D = \infty, Re = 10$)

FVM. From the small figure in lower left of Figure 1, we can see that the wall vorticity of the LBGK solution has small discrepancy with that of the FVM. That is because in LBGK, to get wall vorticity, the finite difference method has to be involved and there are only 15 lattices in y, z direction. In Figure 5, the lower right is the pressure drop along the axial line got from the LBGK and FVM solutions. The results agree very well. Here, the pressure drop $\Delta p/(\rho U^2)$ of case $Re = 10$ is higher than other cases with higher Reynolds number and around the stenose ($x = 0$), the pressure drop is very steep. From this case, it is also found that although LBM based on the microscopic kinetic equation, it still can give out accurate results with coarse lattices.

For case of $S/D = \infty$ with Reynolds number 50, results comparison is shown in Figure 6. In Figure 6, we can see that both the normalized axial and radial velocity component U, V profiles in different x positions obtained from LBGK and FVM agree very well. In Figure 7, the axial $U_{\max}$ in axis and pressure along axis got from the two methods also match in high accuracy.

In Figure 8, for Reynolds number 100, comparisons of the normalized axial and radial component velocity at different axial position are performed. The results of LBGK method agree well with that of FVM.

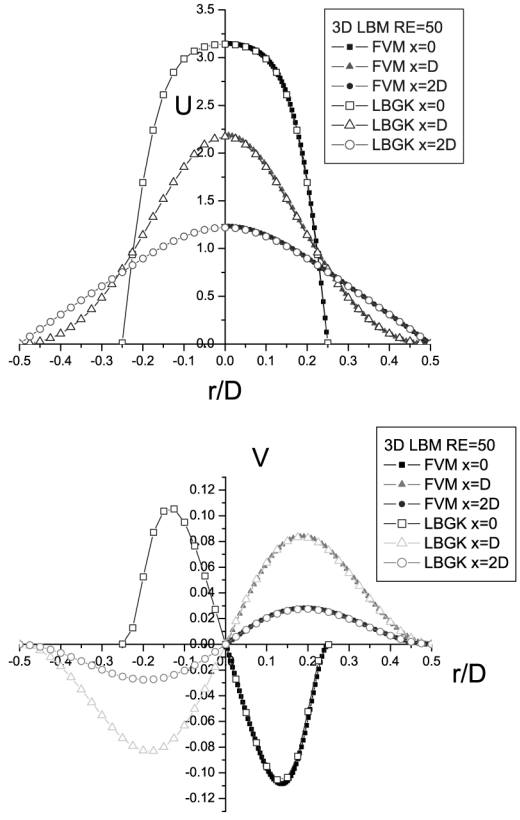

Figure 6.
Axial and radial velocity profiles ($S/D = \infty, Re = 50$)

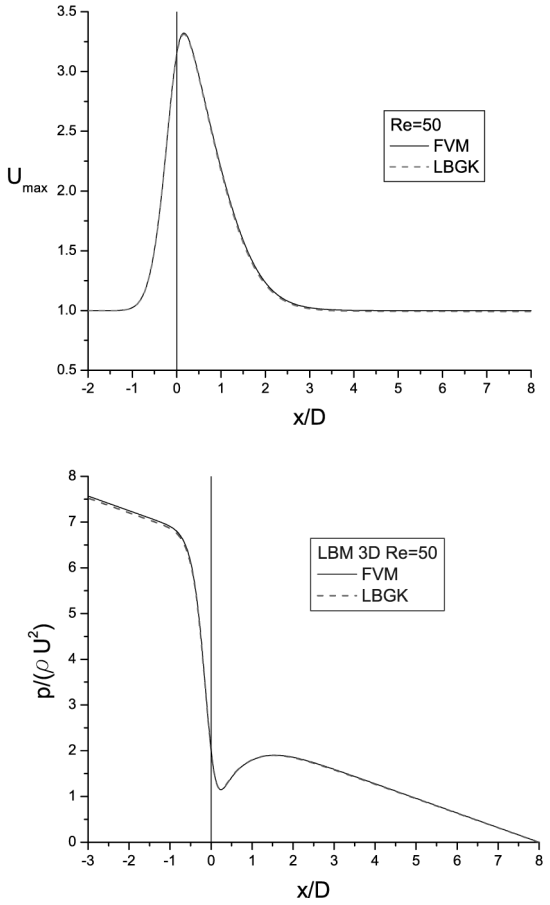

Figure 7.
Axial velocity and pressure along axis $(S/D = \infty, Re = 50)$

After some results of LBGK and FVM are presented and compared, we would like to make a detailed comparison of accuracy and efficiency between the LBGK and FVM solver. For that purpose, three uniform meshes with $N_x \times N_y \times N_z = 111 \times 11 \times 11$(coarse), $221 \times 21 \times 21$(medium) and $441 \times 41 \times 41$(fine) grid nodes are used for LBGK solver to simulate case of $S/D = \infty$. Each finer mesh is obtained by doubling the number of cells of the coarser mesh in each direction. Unstructured linear brick element meshes with equivalent total grid nodes are generated for FVM solver.

The overall order of accuracy of a solution can be estimated using the following formula (Ferziger and Peric, 1999):

$$n \approx \frac{\lg\left(\sum|\phi_{2h} - \phi_{4h}|/N\right) - \lg\left(\sum|\phi_h - \phi_{2h}|/N\right)}{\lg 2} \tag{11}$$

where ϕ represents a dependent variable; N is the total number of points compared; and subscripts h, $2h$, $4h$ stand for solutions on fine, medium, and coarse meshes with grid spacing doubled each time. Here, the accuracy results are presented in terms of

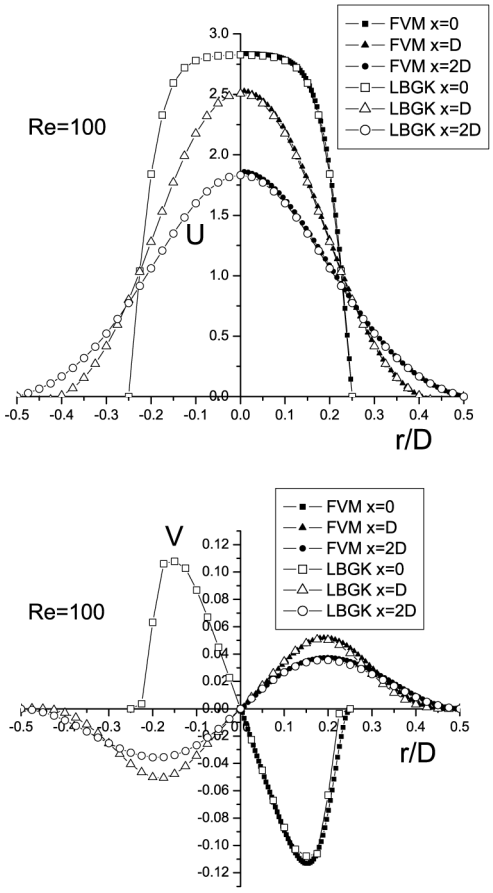

Figure 8.
Axial and radial velocity profiles ($S/D = \infty, Re = 100$)

u-velocity component. With $\phi = u$ in equation (11), the order of accuracy for LBGK solver estimated from the solutions with three meshes is 1.89. The average discretization error of a simulation on mesh h can be estimated via the Richardson extrapolation (Ferziger and Peric, 1999) as:

$$\varepsilon = \frac{\text{Error}}{\sum|\phi_h|/N + \text{Error}} \quad \text{where} \quad \text{Error} \approx \frac{\sum|\phi_h - \phi_{2h}|/N}{2^n - 1} \tag{12}$$

In the above, the denominator in the first equation is the estimated average "exact" solution and n in the second equation is the order of accuracy of the solver (Lai *et al.*, 2001). If equation (12) is used to estimate the average errors on the medium and fine meshes for u velocity, it is found that LBGK solutions have discretizati on errors of about 1.33 and 0.40 per cent.

The efficiency of each solver is evaluated by comparing the respective computing times required. This comparison is not straightforward. To minimize the influence of

computers and convergence criterion, in this study, both the LBGK solver and FLUENT are executed on a super computer (Compaq ES40: total performance of 5,300 Mflops) in the National University of Singapore. The initial conditions of the flow field are also the same. The residual used to monitor the convergence is defined using the u-momentum equation for two solvers, and they are defined as (Lai *et al.*, 2001):

$$\text{LBM}: \quad \sum \left| \frac{u - u^0}{\delta t} \text{vol} \right| \quad \text{and}$$

$$\text{FLUENT}: \quad \sum \left| \left(u\frac{\partial u}{\partial x} + v\frac{\partial u}{\partial y} + w\frac{\partial u}{\partial z} - \nu\left(\frac{\partial^2 u}{\partial x^2} + \frac{\partial^2 u}{\partial y^2} + \frac{\partial^2 u}{\partial z^2} \right) + \frac{\partial p}{\partial x} \right) \text{vol} \right|$$

Note that all the computations are carried out on a single-CPU of the computer Compaq ES40, which does not take parallel advantage of the LBM. In Table I, it seems that the lattice BGK simulation takes about 6-10 times more computing time to obtain the steady-state solutions when compared with FVM (FLUENT).

In the end of this part, we would like to discuss the effect of distance between two adjacent stenoses on streamlines, shear stress, vorticity and velocity distribution as the flow passes through them.

Using LBGK method, we obtained a group of results for $S/D = 2, 3, 4$ with Reynolds number 10, 50 and 150 which is shown in Figures 9-11, respectively. To save mesh points, for $Re = 10$ cases, only 31 lattices in y, z direction are used.

In Figures 9-11, the streamlines are illustrated above the axis and the shear stress contours are below the axis. The shear stress values labelled in figures are normalized by ρU^2, where U is the characteristic velocity. The maximum shear stress value for $Re = 10$, 50 and 150 case are about 3.59, 0.94 and 0.40, respectively. These streamlines and shear stress distribution are quite consistent with results of FVM. From Figure 9, we can see that at Reynolds number of 10, the streamlines and shear stress contours for $S/D = 2, 3, 4$ are similar (case of $S/D = 4$ did not show here). The flow around each constriction almost has no interference with other.

In Figure 10, cases of Reynolds number 50 illustrated. The streamlines and shear stress contours for $S/D = 3$ and 4 are similar. The shear stress contours demonstrated that for case $S/D = 2$, there are weak interference. The streamlines in cases of $Re = 50$ indicated that flow separated and very small eddies formed behind the stenoses.

In Figure 11, we can see that when Reynolds number is 150, between the two constrictions, there is a circulation zone which fills most part of the valley region. The shear stress fields are altered and the recirculatory eddy from the upstream constriction is spread downstream and affects the flow passing through the downstream constriction. In case of $S/D = 2$, there is a separation streamline that

Solver	Coarse mesh	Medium mesh	Fine mesh
LBGK simulation	4.3 (3,600)	80.8 (8,947)	2.101 (21,240)
FVM(FLUENT)	0.5 (30)	6.2 (120)	323.2 (370)

Note: Comparison of CPU times in minutes to get 3 order of residual reduction for steady flow through constricted tube ($S/D = \infty, Re = 10$) (number in parentheses is the number of steps)

Table I.

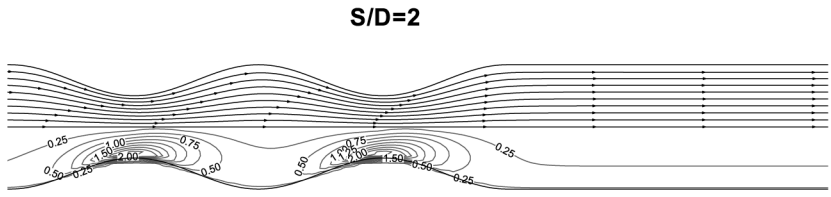

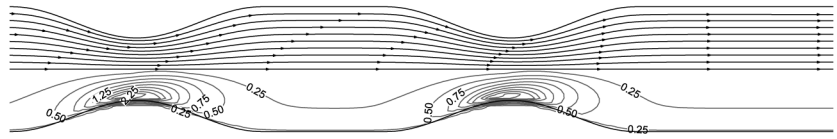

Figure 9.
Streamlines and shear stress contours ($Re = 10$)

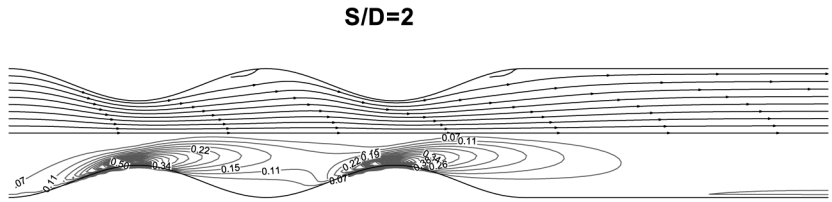

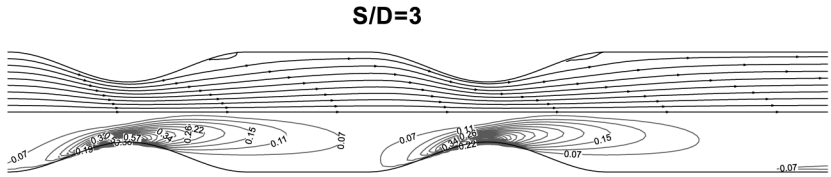

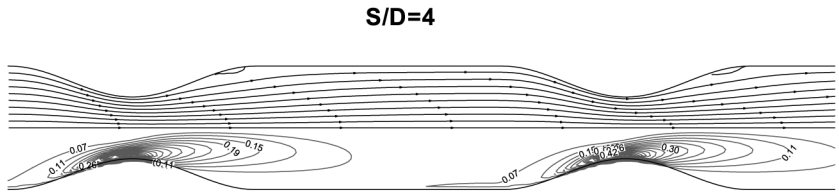

Figure 10.
Streamlines and shear stress contours ($Re = 50$)

divides the flow into two parts: the recirculating flow field between two constrictions and the main flow field near the centre of the tube with relatively straight and parallel streamlines.

The variations of the axial velocity and wall vorticity due to the influence of the constriction spacing ratios and Reynolds number is shown in Figures 12 and 13,

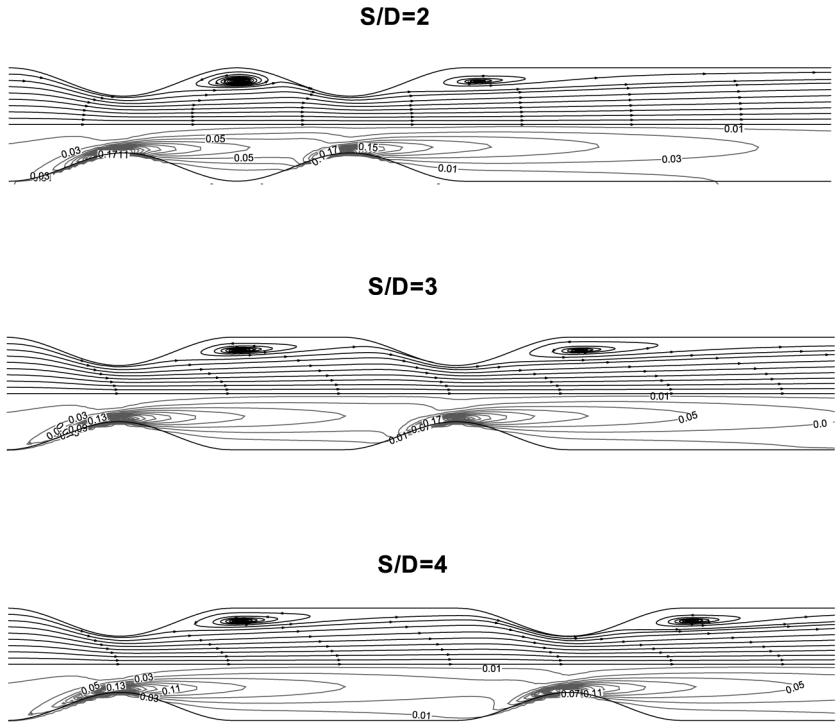

Figure 11.
Streamlines and shear stress contours ($Re = 150$)

respectively. In Figure 12, it is obvious that the maximum centreline axial velocity does not occur at the throat because at that point, the fluid is still in acceleration and actually the maximum axial velocity occurs slightly downstream of each of the constrictions. When Reynolds number is 150 and $S/D = 2, 3$, the maximum velocity value near the second constriction is also slightly higher than the maximum value at the first constriction because the flow interference between the double constrictions exists. For $Re = 150$, $S/D = 4$ case and all of $Re = 50$ or 10 cases, the flow interference is very weak and the maximum velocity values near the two constrictions are almost same.

For the wall vorticity, the magnitude of the wall vorticity value increase rapidly when the flow approaches the constriction and reaches a peak value slightly before the throat position. At a location downstream of the peak value the wall vorticity decrease rapidly and will reverse to negative value when the separation begins at the wall of the tube. It is also obvious that the peak wall vorticity value increases with increasing Reynolds number. When $Re = 150$, $S/D = 2$ or 3, the flow interference exists. In those cases, the second peak wall vorticity values are always lower than the first ones. However, for other cases, the flow interference is very weak and the two peak values are almost the same.

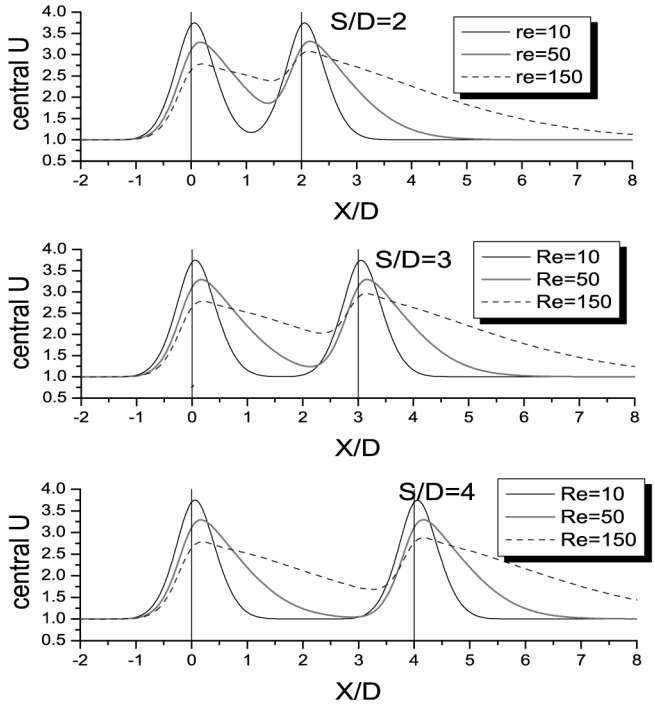

Figure 12.
Variation of axial velocity on axis for different constriction spacings

4. Conclusion

In this paper, fully 3D simulations of flow through tubes with double constrictions are performed through applying a LBGK incompressible D3Q19 model. The numerical results are obtained for a Reynolds number 10-150 with constriction spacing ratios of 2, 3, 4 and ∞.

Firstly, we observed the highly axisymmetric property of the 3D flow in the constricted vascular tube. Some solutions of LBGK and FVM are presented and compared. The velocity profiles, central velocity and pressure drop, etc. obtained from LBGK method are quite consistent with that of FVM.

Then the overall order of accuracy of the LBGK solution is evaluated as around 1.89. In case of $Re = 10$, the average discretization errors of LBGK solution (equation (12)) on the medium ($221 \times 21 \times 21$) and fine ($441 \times 41 \times 41$) meshes is found to be about 1.33 per cent and 0.40 per cent. The efficiency of LBGK solver is also compared with that of FVM. It is found for above cases, the lattice BGK simulation takes about 6-10 times more computing time to obtain the steady-state solutions when compared with FVM solver (FLUENT).

In our study, the 3D steady flows through vascular tubes with double constrictions are investigated in detail. In cases of Reynolds number higher than 50, the maximum velocity on axis shifts downstream, and the maximum value at the second constriction is also higher than the maximum value at the first constriction. The local wall vorticity reaches its highest value slightly upstream of each of the constrictions, and if the flow interference between the two constrictions exists, the first peak wall vorticity value is

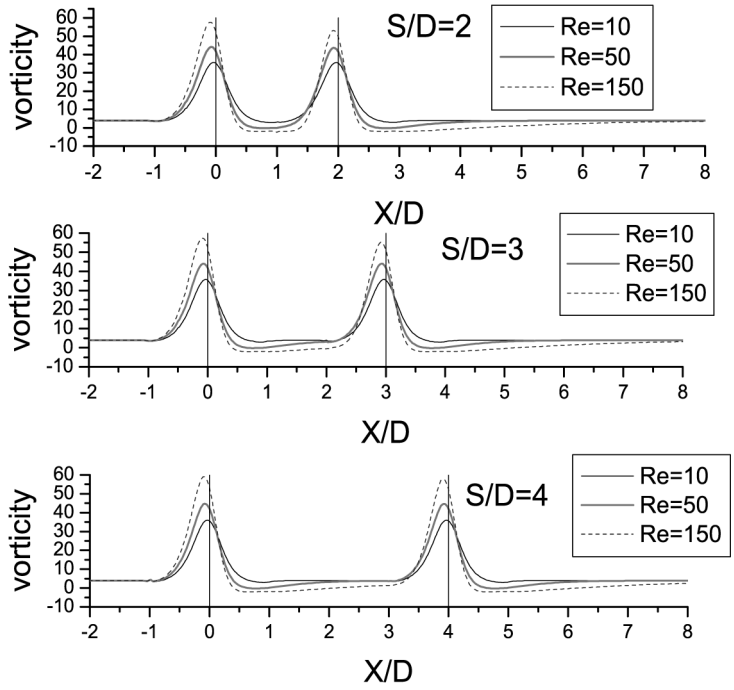

Figure 13.
Variation of wall vorticity for different constriction spacings

always higher than the second peak value. These conclusions are consistent with results obtained by Lee (1994).

All the above results demonstrated that the incompressible D3Q19 model with the curved boundary condition treatment proposed by Bouzidi *et al.* (2001) can handle the problems of 3D steady flow through complex geometry. LBGK method is a useful tool to investigate the steady flow in vascular tubes.

Further studies such as investigating the flow in vascular tube with higher Reynolds number and applying advanced axisymmetric D2Q9 model to investigate the axisymmetric flow are still needed.

References

Artoli, A.M., Hoekstra, A.G. and Sloot, P.M.A. (2002), "3D pulsatile flow with the Lattice Boltzmann BGK method", *Int. J. Mod. Phys. C*, Vol. 13 No. 8, pp. 1119-34.

Bouzidi, M., Firdaouss, M. and Lallemand, P. (2001), "Momentum transfer of a Boltzmann-lattice fluids with boundaries", *Phys. Fluids*, Vol. 13 No. 11, pp. 3452-9.

Chen, H., Chen, S. and Matthaeus, W.H. (1992a), "Recovery of the Navier-Stokes equations using a lattice-gas Boltzmann methods", *Phys. Rev. A*, Vol. 45 No. 8, pp. 5339-42.

Chen, S., Martinez, D. and Mei, R. (1996), "On boundary conditions in Lattice Boltzmann methods", *Phys. Fluids*, Vol. 8 No. 9, pp. 2527-36.

Chen, S., Wang, Z., Shan, X. and Doolen, G.D. (1992b), "Lattice Boltzmann computational fluid dynamics in three dimensions", *J. Stat. Phys.*, Vol. 68, pp. 379-400.

Cosgrove, J.A., Buick, J.M., Tonge, S.J., Munro, C.G., Greated, C.A. and Campbell, D.M. (2003), "Application of the Lattice Boltzmann method to transition of oscillatory channel flow", *J. Phys. A: Math. Gen.*, Vol. 36, pp. 2609-20.

d'Humieres, D., Ginzburg, I., Krafczyk, M., Lallemand, P. and Luo, L.S. (2002), "Multiple-relaxation-time Lattice Boltzmann models in three dimensions", *Philosophical Transactions of the Royal Society of London. Series A: Mathematical Physical and Engineering Sciences*, Vol. 360 No. 1792, pp. 437-51.

Damodaran, V., Rankin, G.W. and Zhang, C. (1996), "Numerical study of steady laminar flow through tubes with multiple constrictions using curvilinear co-ordinates", *Int. J. Numer. Meth. Fluids*, Vol. 23 No. 10, pp. 1021-41.

Ferziger, J.H. and Peric, M. (1999), *Computational Methods for Fluid Dynamics*, Springer, New York, NY.

Filippova, O. and Hanel, D. (1998), "Grid refinement for Lattice-BGK methods", *J. Comp. Phys.*, Vol. 147 No. 1, pp. 219-28.

Guo, Z., Zheng, C. and Shi, B. (2002a), "An extrapolation method for boundary conditions in Lattice Boltzmann method", *Phys. Fluids*, Vol. 14 No. 6, pp. 2007-10.

Guo, Z., Zheng, C. and Shi, B. (2002b), "Non-equilibrium extrapolation method for velocity and pressure boundary conditions in the Lattice Boltzmann method", *Chinese Phys.*, Vol. 11 No. 4, pp. 366-74.

Halliday, I., Hammond, L.A., Care, C.M., Good, K. and Stevens, A. (2001), "Lattice Boltzmann equation hydrodynamics", *Phys. Rev. E*, Vol. 64 No. 1, Art. No. 011208, Part 1.

He, X. and Luo, L.S. (1997), "Lattice Boltzmann model for the incompressible Navier-Stokes equation", *J. Stat. Phys.*, Vol. 88 Nos 3/4, pp. 927-44.

He, X., Luo, L.S. and Dembo, M. (1996), "Some progress in Lattice Boltzmann method: Part I. Nonuniform mesh grids", *J. Comp. Phys.*, Vol. 129 No. 2, pp. 357-63.

He, X., Zhou, Q., Luo, L.S. and Dembo, M. (1997), "Analytical solutions of simple flows and analysis of non-slip boundary conditions for the Lattice Boltzmann BGK model", *J. Stat. Phys.*, Vol. 87, pp. 115-36.

Higuera, F. and Jimenez, J. (1989), "Boltzmann approach to lattice gas simulations", *Europhys. Lett.*, Vol. 9 No. 7, pp. 663-8.

Hou, S.L., Zou, Q., Chen, S.Y., Doolen, G. and Cogley, A.C. (1995), "Simulation of cavity flow by the Lattice Boltzmann method", *J. Comp. Phys.*, Vol. 118 No. 2, pp. 329-47.

Ladd, A.J.C. (1994), "Numerical simulation of particular suspension via a discretized Boltzmann equation. Part 2: Numerical results", *J. Fluid Mech.*, Vol. 271, pp. 311-39.

Lai, Y., Lin, C. and Huang, J. (2001), "Accuracy and efficiency study of Lattice Boltzmann method for steady-state flow simulation", *Numer. Heat Tr. B-Fund*, Vol. 39 No. 1, pp. 21-43.

Lallemand, P. and Luo, L.S. (2003), "Lattice Boltzmann methods for moving boundaries", *J. Comp. Phys.*, Vol. 184, pp. 406-21.

Lee, T.S. (1990), "Numerical studies of fluid flow through tubes with double constrictions", *Int. J. Numer. Meth. Fluids*, Vol. 11 No. 8, pp. 1113-26.

Lee, T.S. (1994), "Steady laminar fluid flow through variable constrictions in vascular tubes", *J. Fluid Eng-T ASME*, Vol. 116 No. 1, pp. 66-71.

Luo, L.S. (1997), "Symmetry breaking of flow in 2D symmetric channels: simulations by Lattice-Boltzmann method", *Int. J. Mod. Phys. C.*, Vol. 8 No. 4, pp. 859-67.

McNamara, G. and Zanetti, G. (1988), "Use of the Boltzmann equation to simulate Lattice-gas automata", *Phys. Rev. Lett.*, Vol. 61 No. 20, pp. 2332-5.

Maier, R.S., Bernard, R.S. and Grunau, D.W. (1996), "Boundary conditions for the Lattice Boltzmann method", *Phys. Fluids*, Vol. 8 No. 7, pp. 1788-801.

Mei, R., Luo, L.S. and Shyy, W. (1999), "An accurate curved boundary treatment in the Lattice Boltzmann method", *J. Comp. Phys.*, Vol. 155 No. 2, pp. 307-30.

Mei, R., Yu, D. and Shyy, W. (2002), "Force evaluation in the Lattice Boltzmann method involving curved geometry", *Phys. Rev. E.*, Vol. 56 No. 4, Art. No. 041203 Part 1.

Mei, R., Shyy, W., Yu, D. and Luo, L.S. (2000), "Lattice Boltzmann methods for 3D flows with curved boundary", *J. Comp. Phys.*, Vol. 161 No. 2, pp. 680-99.

Noble, D.R., Georgiadis, J.G. and Buckius, R.O. (1996), "Comparison of accuracy and performance for Lattice Boltzmann and finite difference simulations of steady viscous flow", *Int. J. Numer. Meth. Fluids*, Vol. 23 No. 1, pp. 1-18.

Peng, Y., Shu, C. and Chew, Y.T. (2004), "A 3D incompressible thermal Lattice Boltzmann model and its application to simulate natural convection in a cubic cavity", *J. Comp. Phys.*, Vol. 193 No. 1, pp. 260-74.

Young, D.F. and Tsai, F.Y. (1973), "Flow characteristics in models of arterial stenoses – I. Steady flow", *J. Biomech.*, Vol. 6 No. 4, pp. 395-410.

Yu, D., Mei, R., Luo, L. and Shyy, W. (2003), "Viscous flow computations with the method of Lattice Boltzmann equation", *Prog. Aerosp. Sci.*, Vol. 39 No. 5, pp. 329-67.

Zou, Q. and He, X. (1997), "On pressure and velocity boundary conditions for the Lattice Boltzmann BGK model", *Phys. Fluids*, Vol. 9 No. 6, pp. 1591-8.